Vol. 17, No. 3 (2018) 1135-1146

Catálisis, cinética y reactores

Revista Mexicana de Ingeniería Química

ADVANCED OXIDATION TECHNOLOGIES TO REMOVE ENDOCRINE DISRUPTORS IN WATER EFFLUENTS BASED ON ZINC SUPPORTED MESOPOROUS CATALYSTS

TECNOLOGÍAS DE OXIDACIÓN AVANZADA PARA REMOVER DISRUPTORES ENDOCRINOS EN EFLEUNTES DE AGUA BASADOS EN CATALIZADADORES MESOPOROSOS SOPORTADOS EN ZINC

P.M. Carraro[1,2], T.B. Benzaquén[1], O.M. Alfan[3], M.I. Oliva[2], G.A. Eimer[1*]

[1] *CITeQ-UTN-CONICET, Universidad Tecnológica Nacional-Facultad Regional Córdoba. Maestro López esq. Cruz Roja s/n, Córdoba, Argentina.*

[2] *IFEG - CONICET, Universidad Nacional de Córdoba. Medina Allende s/n, Córdoba, Argentina.*

[3] *INTEC - CONICET, Universidad Nacional del Litoral. Ruta Nac. N 168 km, Santa Fe, Argentina.*

Received: February 22, 2018; Accepted: April 18, 2018

Abstract

Mesoporous silica material type MCM-41 was modified with different amounts of Zn (1 - 15 wt.%) by the wet impregnation method. Support and catalysts were characterized by means of powder X-ray diffraction (XRD), N_2 nitrogen adsorption-desorption, transmission electron microscopy (TEM), X-ray photoelectron spectroscopy (XPS) and ICP-OES techniques. The Zn-modified mesoporous silicates have been successfully tested for the degradation in aqueous solutions of different endocrine-disrupting (EDs), such as herbicides (atrazine), compounds derived from the plastic industry (bisphenol A) and from the pharmaceutical industry (clofibric acid). The results showed that the Zn/M(5) catalyst exhibited the highest activity. The high performance of this material indicates that the heterogeneous photo-Fenton-like reaction appears as a very promising pre-treatment capable of enhancing the biodegradability of water contaminated with biorecalcitrant chemicals, as the most endocrine disruptors.

Keywords: MCM-41, Zn, advanced oxidation process, endocrine disruptors.

Resumen

Materiales mesoporosos del tipo MCM-41 fueron modificados por el método de impregnación húmeda con diferentes cargas de Zn (1 - 15 % p/p). El soporte y los catalizadores fueron caracterizados por difracción de rayos X (DRX), adsorción-desorción de N_2, microscopia electrónica de transmisión (TEM), espectroscopia de fotoelectrones emitidos por rayos X (XPS) y técnica de ICP-OES. Los silicatos mesoporosos modificados con Zn se evaluados exitosamente en la reacción de degradación en solución acuosa de diferentes disruptores endocrinos (EDs), tales como herbicidas (atrazina), compuestos derivados de la industria plástica (bisfenol A) y de la industria farmacéutica (ácido clofíbrico). Los resultados mostraron que el catalizador Zn/M(5) exhibió la mayor actividad. La mejor performance de este material indica que la reacción heterogénea foto-Fenton aparece como un pretratamiento muy prometedor, capaz de mejorar la biodegradabilidad de aguas contaminadas con productos químicos biorecalcitrantes, como la mayoría de los disruptores endocrinos.

Palabras clave: MCM-41, Zn, procesos avanzados de oxidación, disruptores endocrinos.

1 Introduction

For many years, water pollution has been generated by human alteration of natural environments. Some toxic and carcinogenic compounds found in polluted waters are known as endocrine disruptors (EDs). An endocrine-disrupting compound was defined by the U.S. Environmental Protection Agency (EPA) as "an exogenous agent that interferes with synthesis, secretion, transport, metabolism, binding action or elimination of natural blood-borne hormones that are present in the body and are responsible for homeostasis, reproduction, and developmental process" (Diamanti-Kandarakis *et al*. 2009; USEPA 2001).

* *Corresponding author. E-mail*: geimer@frc.utn.edu.ar
Tel. +54 0351 4690585, Fax +54 0351 4690585
doi: 10.24275/uam/izt/dcbi/revmexingquim/2018v17n3/Carraro
issn-e: 2395-8472

Among these are includes pesticides, persistent organochlorines and organohalogens, alkyl phenols, heavy metals, phytoestrogens, synthetic and natural hormones, as well as medicines, pharmaceuticals and personal care products (PPCPs).

On the one hand, the herbicide atrazine (ATZ, 2-chloro-4-(ethylamine)-6- (isopropylamine)-s-triazine) is a widely used pesticide in the world. As a result, this herbicide is one of the most commonly detected pesticide contaminant of ground, surface, and drinking water. ATZ is also potent endocrine disruptor that is active at low ecologically relevant concentrations (Benzaquén *et al*. 2013).

On the other hand, Pharmaceutical and Personnel Care Products (PPCPs) continues to grow worldwide on par with many agrochemicals (Esplugas et al 2007). Typical sources are sewage effluents and hospital and animal waste, which contain a variety of PPCPs. Clofibric acid (CA, 2-(4-Chlorophenoxy)-2-methylpropionic acid) is the main pharmacologically active metabolite of the lipid lowering drug, clofibrate. Numerous studies have demonstrated the occurrence of CA in surface, groundwater and even drinking water (Tixier *et al*. 2003).

In addition, Bisphenol A (BPA, 2,2-(4,4'-dihydroxydiphenyl) propane) is a chemical widely used in the plastics industry. It is also a well-known as an endocrine disruptor and can be the cause of different diseases (Huang *et al*. 2011). Unfortunately, BPA cannot be entirely removed from water solutions by conventional treatments.

The potential effects of these emergent contaminants in water are still uncertain and further investigation is needed to improve their efficient removal from water. Advanced Oxidation Processes (AOPs) are efficient and effective technology for water treatment that allow the total or partial removal of recalcitrant organic pollutants resistant to conventional treatments (Benzaquén *et al*. 2013; Pignatello *et al*. 2006; Benzaquén *et al*. 2015). Among the various AOPs, heterogeneous Fenton like process in combination with UV-vis light is highly efficient in wastewater treatment. These processes involve the generation of the hydroxyl free radical, which has a very high oxidation potential, by means of the use of strong oxidants (H_2O_2), radiation ultraviolet, and catalysts (Benzaquén *et al*. 2015; Chu *et al*. 2007). The so-called heterogeneous Fenton-like systems use a solid catalyst in the presence of hydrogen peroxide. Some semiconductor oxides can be used in the AOPs applications due to its transition metal ions (such as Zn) tend to decompose the H_2O_2, generating free radicals at low pH values. This aspect results very attractive for increase the process efficiency (Liotta *et al*. 2009; Jones 1999). Among them, ZnO zinc oxide (band gap of 3.37 eV) is considered a good alternative in comparison to other commonly used photo-catalysts (such as TiO_2) (Lee *et al*. 2015; Ansari *et al*. 2013; Huang *et al*. 2015). This oxide possesses a high chemical stability, good photo and piezoelectric behavior and excellent photocatalytic activity at room temperature, besides being cheap and non-toxic (Chandrappa *et al*. 2012), and producing electronic transitions in the UV-A ultraviolet range (Litter 2005). In this way, ordered silicate mesoporous materials, like MCM-41, have received widespread interest as supports for such oxide species. Thus, MCM-41 offers unique structure, high surface area and porous structure, which allows their modification by means of the transition metal incorporation obtaining efficient photocatalytic systems. Thereby, mesoporous structures modified with Zn constitute an important alternative to be used as photocatalysts for water treatment (Mihai *et al*. 2010).

The aim of present study was to synthesize mesoporous molecular materials (MCM-41) with different zinc loadings, for their utilization in the degradation of different EDs in aqueous medium by heterogeneous photo-Fenton process.

2 Materials and methods

2.1 Synthesis

The pure siliceous mesoporous material (MCM-41) was synthesized as previously reported (Elías *et al*. 2009) following the method B, using cetyltrimethylammonium bromide (CTAB, Merck 99%) as template, tetraethoxysilane (TEOS, Aldrich 98%) as silicon source and sodium hydroxide (NaOH) aqueous solution 2 M for hydrolysis and pH adjustment. The molar composition of gel was: NaOH/Si = 0.50, surfactant/Si = 0.12, H_2O/Si = 132. In a usual synthesis, CTAB was dissolved in water - NaOH solution at 313 K; this new solution was then cooled to room temperature and TEOS was finally incorporated. The mixture was vigorously stirred for 4 h at room temperature and then for 3 h at 343 K in a closed flask.

The final solid was filtered, washed and dried at 333 K overnight. To remove the template, the samples were heated (heating rate of 2 K/min) under N_2 flow

up to 773 K for 6 h and then calcined at the same temperature under air flow for 6 h.

Zn/MCM-41 molecular sieves were modified with different Zn loadings (1 - 15 wt.%) by the wet impregnation method. The MCM-41, previously calcined at 773 K, was added to an aqueous solution of $Zn(NO_3)_2 \bullet 6H_2O$ (Anedra 99.2 %) with a concentration corresponding to the desired metallic loading. Then, the water was slowly removed by rotary evaporation at 323 K for about 30 min. The resulting powder was dried at 333 K and then calcined for 9 h at 773 K. The resulting materials were named Zn/M(x), where x indicates the expected metal loading percentage (nominal loading).

2.2 Characterization

The textural characterization was carried out by N_2 adsorption - desorption isotherms at 77 K (N_2 with 99.999% purity) was conducted in Micromeritics ASAP 2000. The samples were previously vacuum-degassed at 573 K for 12 h. From the N_2 adsorption - desorption data obtained for each catalyst and support, specific surface was calculated by the Brunauer-Emmett-Teller (S_{BET}) method in the pressure range of p/p0: 0.01 - 0.25 (Brunauer *et al*. 1938) and the total pore volume (V_{TP}) was obtained by the Gurvich's rule (Rouquerol *et al*. 1999). The pore size distributions were determined by NLDFT method, for SiO2 cylindrical pores in the adsorption branches (Ravikovitch *et al*. 2001). The structure of the samples was analyzed by X-ray powder diffraction (XRD) using Cu Kα radiation (λ = 1.5418 Å), measured with a PANalytical X'Pert PRO diffractometer. The XRD patterns where obtained in 2θ range from 1.5 to 7º and from 10 to 80º. Moreover, the solids were analyzed by Transmission Electron Microscopy (TEM) with a JOEL JEM-1200 EX II, working voltage: 120 kV. A small drop of the dispersion (sample in solution water-ethanol 50 %) was deposited on copper grid and then evaporated in air at room temperature. The Zn content was determined by Inductively Coupled Plasma Atomic Emission Spectroscopy (ICP) using a spectrophotometer VISTA-MPX CCD Simultaneus ICP-OES-VARIAN. The samples were previously digested with HF and HNO_3. X-ray photoelectron spectra (XPS) were performed on a multi-technical system (SPECS) equipped with a dual X-ray source Mg/Al model XR50, which has a hemispheric analyzer PHOIBOS 150 operating in fix analyzer transmission mode (FAT). Spectra were acquired with step energy of 30 eV, using Mg Kα radiation X-ray source operated at 100 W. Work pressure in analysis chamber was lower than 2.10-8 mbar. Binding energy values were corrected using as reference the adventitious C 1s line at 284.6 eV. UV-Vis diffuse reflectance spectra (UV-Vis DRS) were performed on Jasco 650 spectrometer with an integrating sphere in the wavelength range of 200e900 nm. After the reaction, the total Zn leaching into the reaction mixture was measured by atomic absorption spectroscopy (AAS) using a SHIMADZU AA - 7000 series.

2.3 Chemicals

ATZ ($C_8H_{14}ClN_5$, ≥ 90%, SYNGENTA), BPA ($C_{15}H_{16}O_2$, ≥ 90%, Aldrich) and CA ($C_{10}H_{11}ClO_3$, > 97%, Aldrich) were chosen as the model endocrine disruptors. Hydrogen peroxide (H_2O_2, 30% w/v solution, Ciccarelli p.a) were used as photo-Fenton reagents.

2.4 Experimental setup

Photo-Fenton like experiments were carried out in a batch system consisting of a borosilicate glass tubular reactor, illuminated with four UV-Vis lamps (ACTINIC BL 20, Philips). Each lamp, with emission in the UV and visible range (350-400 nm, with two bands at 404 and 438 nm), was placed at the focal axis of a reflector. The volume of the reactor was 500 mL (VT). The isothermal condition (25 °C) was achieved by the incorporation of an all-glass heat exchanger connected to a thermostatic bath. The reactor included a sintered glass piece placed at the bottom through which an air flow was introduced to provide good mixing conditions (see supporting information for a schematic representation of the photoreactor).

The incident radiation flux at the reactor window, experimentally measured by ferrioxalate actinometry (Murov *et al*. 1993) was $6.96 \times 10\text{-}9$ Einstein $cm^{-2}s^{-1}$.

2.5 Heterogeneous photo-Fenton experiments and analytical methods

To prepare the reacting solution, 15 mg of ED were placed in a volumetric flask. Distilled water was then added to dissolve the pollutant, and the resultant solution was diluted to a total volume of 500 mL. This initial concentration of the pollutant, C0ED, is the value expected in wastewater to be treated. Experimental run began when the suspended catalyst in contaminant solution was mixed in the dark, for 60 min, to achieve the adsorption/desorption equilibrium

between ED and the catalyst. During this time, the solution was saturated with air by intense bubbling and the reactor lamps were turned on to stabilize the radiation emission. After this period, when the system was stabilized and the adsorption equilibrium was reached, the required amount of H_2O_2 solution was added, the ED aqueous solution was incorporated in the photoreactor and the first sample was taken from the reactor (t = 0), to start the irradiated experiment. Each experiment lasted 240 min, and liquid samples were taken at equal time intervals and properly filtered.

ATZ, BPA and CA concentrations were measured by HPLC (Perkin Elmer, Series 200) using reverse phase liquid chromatography equipped with a UV detector and a C18 column (Waters), the eluent flow rate was 1 mL min^{-1}. The chromatographic conditions adopted in the quantification of each of these compounds were:

(i) ATZ, the eluent was a binary mixture of distilled water and methanol (proportion 40:60) and the detection was performed at 221 nm (Benzaquén *et al*. 2017).

(ii) BPA, the eluent used was a binary mixture of distilled water and acetonitrile (proportion 50:50) and the detection was performed at a wavelength of 278 nm (Manassero *et al*. 2013).

(iii) CA, the mobile phase was a binary mixture of acidified water (with 0.1% v/v phosphoric acid) and acetonitrile (50:50) and the absorbance detection was made at 227 nm (Dordio *et al*. 2009).

Hydrogen peroxide concentration was analyzed by means of a modified iodometric technique using a UV-VIS Jasco V-650, at 350 nm (Allen *et al*. 1952). For each pollutant, a set of experimental runs for heterogeneous photo-Fenton-like reactions was performed, using the different synthesized catalysts. All experiments were performed at the same initial concentration of ED, catalyst initial concentration (C^0_{CAT}), H_2O_2 to the ED initial molar ratio ($R = C^0H_2O_2/C^0_{ED}$), radiation levels and pH. It should be mentioned that, the effect of these parameters was studied in previous experiments and the optimal degrading conditions were determined (Benzaquén *et al*. 2017). The operating conditions are summarized in Table S1 (see supporting information).

3 Results and discussion

3.1 Chemical-physical, structural and morphological characterization

N_2 adsorption - desorption isotherms carried out for the studies materials are illustrated in Fig. 1.a. As it can be observed, the isotherms of the support and the Zn/MCM-41 samples belong to type IV of IUPAC classification, which are typical of mesoporous structures (Everett 1971; Torres-Otáñez *et al*. 2017). The isotherms of the support and the Zn/M(1) show identical shapes and exhibit a sharp increase in the inflection region at a relative pressure around p/p0 = 0.1 to 0.25, characteristic of a narrow step of capillary condensation inside the primary mesopores.

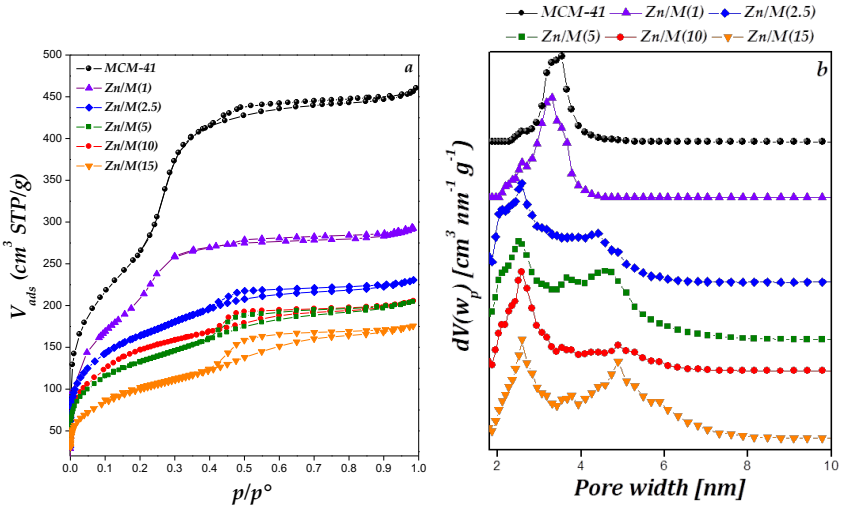

Fig. 1. Nitrogen adsorption-desorption isotherms (a) and NLDFT pore size distribution (b) of catalyst.

Table 1. Structure, textural and chemical properties of MCM-41 and Zn/MCM-41 materials.

Sample	a_0 (nm)[a]	S_{BET} (m^2/g)[b]	$\mathbf{V_{TP}}$ (cm3/g)[c]
MCM-41	4.06	940	0.70
Zn/M(1)	4.00	764	0.42
Zn/M(2.5)	3.94	592	0.36
Zn/M(5)	3.86	480	0.32
Zn/M(10)	3.94	532	0.32
Zn/M(15)	4.01	370	0.27

[a] $a_0 = (2/\sqrt{3})d_100$. [b] Determined by BET. [c] Pore volume. (V_{TP}) determined by N_2 adsorption-desorption.

However, the Zn/M(1) sample has lower adsorption capacity than support, which would evidence that throughout the impregnation treatment, the support structure remains unchanged, although some pores could become blocked to the nitrogen access.

The others Zn/MCM-41 materials display similar shapes to that for MCM-41, however, the inflection it is less pronounced and the adsorption capacity decreases with Zn loading increasing. Such soft inflection provides clear evidence of a broadly pore diameter range for these materials, as it can be seen in Fig. 1.b, according also with a decrease of structural order. Probably, the presence of clusters and/or small nanoparticles of ZnO oxides, as well as large nanoparticles on the external surface could affect the pore structure and the textural properties of these materials. The Zn/M(15) isotherm display similar shape to that for MCM-41, showing an important hysteresis loop Type H4. The close of the hysteresis loop is due to a percolation phenomenon produced by a pore blocking caused by structural defects on the mesopores of the material (García Blanco *et al*. 2011).

Fig. 1.b shows the pore size distribution (PSD) of the catalysts and the support, calculated by Non local Density Functional Theory (NLDFT), using adsorption branch. The MCM-41 and Zn/M(1) samples have uniform and narrow pore size distribution, with pore size of approximately 3.5 nm. However, the Zn/MCM-41 samples with more of 1% wt. of Zn, evidence a maximum value for pore size close at 2.6 nm, indicating the primary mesopore presence, with an important contribution of larger pore sizes (4-6 nm). Therefore, the zinc loading samples present a bimodal PSD, possibly as a result of the partial blockage of the primary mesopores with the increased zinc oxide amount, the subsequent deterioration of structure and appearance of larger size pores with irregular distribution (Rouquerol *et al*. 1999; Do *et al*. 2005).

Table 1 summarizes the textural and structural properties of the different samples prepared in this study. As it is observed, Zn/MCM-41 samples present a decrease of S_{BET} and pore volume values in comparison with MCM-41, combined with a broadening of the diameter distribution. This fact is attributed to the mentioned structural deterioration with the Zn loading increasing.

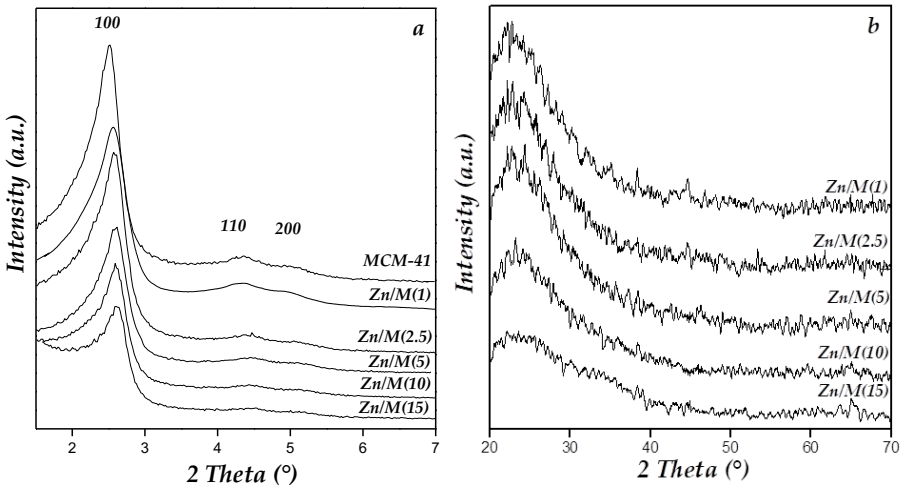

Fig. 2. Low-angle XRD patterns (a) and high-angle XRD patterns (b) of catalyst.

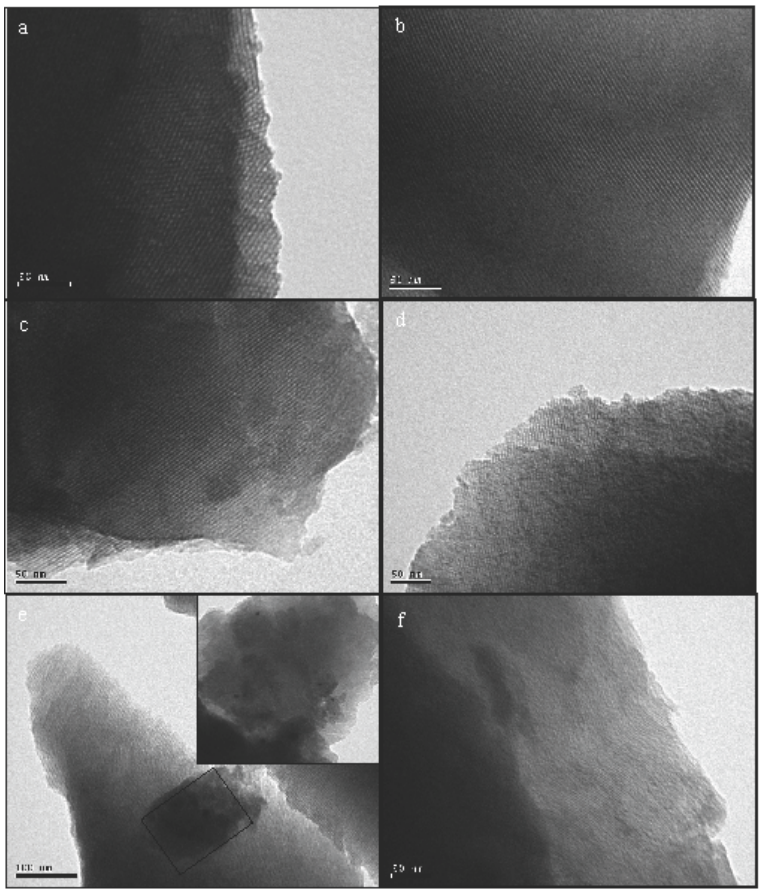

Fig. 3. Transmission electron microscopy images of (a) MCM-41, (b) Zn/M(1), (c) Zn/M(2.5), (d) Zn/M(5), (e) Zn/M(10) and (f) Zn/M(15).

The low-angle XRD patterns of the synthesized catalysts and the support are shown in Fig. 2.a. Three diffraction peaks are clearly observed for the MCM-41 support. The first diffraction peak corresponds to plane (100) of the 2D-hexagonal structure of MCM-41 materials, and two weak reflections ascribed to (110) and (200) (Do *et al*. 2005, Vaschetto *et al*. 2018). The low-angle XRD patterns of the zinc loaded samples are similar to that of the pure MCM-41, indicating that the well-ordered pore structure was mainly preserved. However, for the samples with the higher zinc loadings the peaks were broadened and their intensities decreased, indicating that long-range order of Zn/MCM-41 diminished. In addition, it can also be a result of loss of contrast between pores and silica due to filling of the pores by the ZnO.

Moreover, the (100) reflections moved slightly to higher angle and lattice parameter (a_0) decreased concurrently with this decrease in the structural order (Carraro *et al*. 2014). Fig. 2.b depicts the high-angle XRD patterns of the Zn/MCM-41. As it can be seen all of the patterns exhibited the broad amorphous silica peak at around 23º, but no characteristic diffraction peaks of zinc oxide are detected in XRD pattern. Thus, if ZnO species exit these are amorphous or clusters/particles with size below the XRD detection limit (~5 nm). Such zinc species could be finely dispersed inside the mesochannels or on the surface of the MCM-41 support. These results are consistent with some prior reports, where ZnO nanoparticles could not be detected by XRD, in the case of samples with Zn loading lower than 20-25 wt.% (Mihai *et al*. 2010; García Blanco 2011; Lihitkar *et al*. 2012; Jiang *et al*. 2006, Chen *et al*. 2004). Representative transmission electron microscopy images (Fig. 3) of the catalysts were performed in order to elucidate the hexagonal arrangement of mesopores channels as well as ZnO nanoparticles location.

Table 2. Binding energies and surface zinc compositions of Zn/MCM-41(x) samples and reference ZnO.

	Binding Energy (eV)				Zn/Si	Zn (at. %)	Zn bulk (wt.%)	Zn/Si
Sample	**Zn $2p_{3/2}$**	**Zn $2p_{1/2}$**	**O 1s**	**Si 2p**	**(XPS)**	**(XPS)**	**(ICP)**	**(ICP)**
Zn/M(1)	1022.9	1045.7	533.3	103.9	0.003	0.10	0.09	0.0008
Zn/M(2.5)	1022.1	1045.5	533.3	104.2	0.004	0.20	2.65	0.025
Zn/M(5)	1022.4	1045.7	533.4	104.1	0.007	0.20	4.29	0.041
Zn/M(10)	1022.7	1045.6	533.3	103.9	0.013	0.40	9.87	0.100
Zn/M(15)	1023.1	1045.8	533.4	104.2	0.015	0.50	14.6	0.157
ZnO	1020.0	1045.0	530.0	-	-	-	-	-

TEM images of the Zn/MCM-41 samples exhibit uniform, parallel and straight mesochannels, characteristic of the well-defined hexagonal pore arrangement of MCM-41 type materials (Bengoa *et al*. 2005).

It is well known that the darker areas in TEM images represent the electronically more dense phases, thus, metal oxide is considered to be present when irregular contrasts in the images are observed (García Blanco *et al*. 2011; Bengoa *et al*. 2005; Elías *et al*. 2012). Then, the small black spots (Fig. 3.e) over the pore arrangement can be attributed to the presence of ZnO, whose size is about 5 nm (Fig.4.e), nearby to the XRD detection limit (< 4 – 6 nm). This ZnO could be located inside the pores, judging by the broad distribution of pore sizes found. In addition, the absence of ZnO crystalline over the others samples confirms the well dispersion of ZnO in MCM-41. The surface chemical composition, Zn oxidation states and species identification on the Zn/MCM-41 materials have been studied by XPS. The binding energies of the Zn 2p, the O 1s and the Si 2p are presented in Table 2. O 1s and Si 2p spectra of a Zn/MCM-41 sample taken as representative are shown in supporting information. The O 1s peak shows a symmetric peak located around 533 eV, which correspond mainly to the O 1s photoemission of the oxygen atoms presented on the siliceous support (Shen *et al*. 2014). Other peaks of oxygen attributable to ZnO oxide, weakly bound OH^- or water molecules were not observed, probably due to that their low signal is masked by the oxygen of the SiO2. The binding energy of the Si 2p in all the samples was about 104.4 eV, characteristic for the silicates.

Fig. 4 shows the signal of the Zn 2p lines for all the samples. The binding energies for Zn 2p3/2 and Zn 2p1/2 at 1022.8 eV and 1045.7 eV respectively give a spin orbit splitting (SOS) of ~22.9 eV. This corroborates that the Zn exists in the Zn^{+2} chemical state (Dupin *et al*. 2000). In addition, it is known that SOS is sensitive to the chemical environment of Zn. Thus, Carlson 1975 reported that in Zn metal it is 24.6 eV but 22.2 eV in pure ZnO. In our samples, SOS is 22.9 eV, which implicates that the ZnO would be not predominantly as "bulk" ZnO, but probably as ZnO species highly dispersed and interacting with the support surface, according to (Carlson 1975).

In addition, the Table 2 lists the surface Zn/Si atomic ratios and the Zn surface atomic concentrations determined by XPS and the bulk Zn/Si ratios and the Zn bulk concentrations determined by ICP for all of the synthesized catalysts.

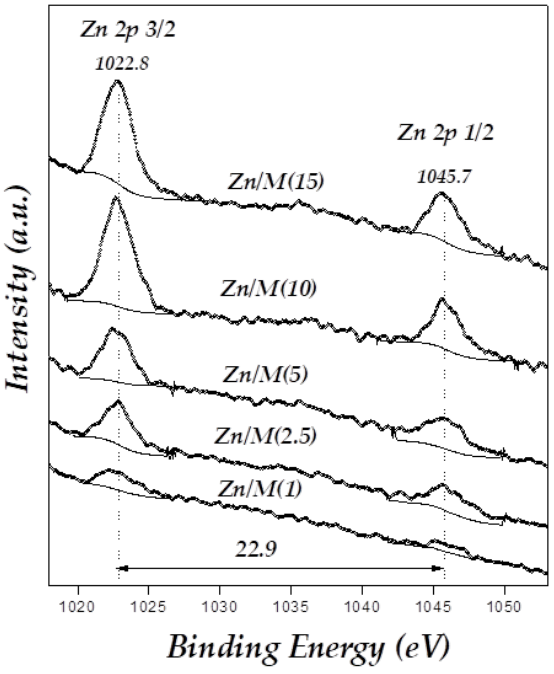

Fig. 4. XPS Zn 2p3/2 and Zn 2p1/2 spectra of Zn-modified MCM-41 samples.

Table 4. ATZ, BPA and CA degradation for each catalytic cycle.

	ATZ degradation (%)	**BPA degradation (%)**	**CA degradation (%)**
1st **cycle**	59.8	81.6	86.8
2nd **cycle**	57.9	82.6	85.9
3rd **cycle**	58.2	80.4	84.9

As it can be seen, the surface Zn/Si ratios are notably lower than the corresponding bulk Zn/Si ratios, indicating that the Zn species would be incorporated inside the mesopores as clusters or very small nanoparticles.

The UV-vis diffuse reflectance spectra for Zn/MCM-41 samples are shown in Fig. 5. The main feature for all of the samples is a single absorption band around 280-380 nm. It is known that the macrocrystalline ZnO starts to absorb close to 370 nm (Zhang *et al*. 2000).

Therefore, the blue-shift in the absorption spectra is corresponding to an increasing band gap of the semiconductor powder which arises from the size quantization effect. Thus, the shift of the absorption edge of semiconductor to lower wavelength is attributed to decreasing particle size. Accordingly, this absorption band increases in intensity and its position shifts to higher wavenumbers with increasing Zn loading, giving account for larger ZnO species.

3.2 Effect of the different metal loadings on the photocatalytic activity

Initially, different types of previous experiments were carried out in order to investigate the effects of initial catalyst concentration (C^0_{CAT}) and H_2O_2 to EDs initial molar ratios (R) and radiation levels (Rad) on the catalytic activity. These runs (results not shown) demonstrated that the oxidation rate was negatively affected by the increase of C^0_{CAT} above 1 g L^{-1} and of H_2O_2 above the ratio R = 175. In addition, efficient pollutants degradation was achieved at the highest incident radiation.

Then, using the annular photoreactor, the feasibility of the different (ATZ, BPA and CA) degradation by the heterogeneous photo-Fenton-like process with diverse zinc modified MCM-41 materials was studied. Five different values of zinc loading were investigated: 1, 2.5, 5, 10 and 15 wt.%, by keeping C^0_{CAT}, R and Rad constant.

Fig. 6.a, 6.b and 6.c illustrate the evolution of ATZ, BPA and CA concentrations, respectively, as a function of the reaction time for different metal loadings, with constant values of H_2O_2 to the EDs initial molar ratio (R = 175), pH=5.5 and catalyst initial concentration (C^0_{CAT} = 1 g L^{-1}). As observed in these figures, when the metal loading increased from 1 to 5 wt.% an increase in the catalytic activity was obtained.

However, samples with higher zinc contents (10 and 15 wt.%) showed an important decrease in the catalytic activity for all the pollutants studied. This behavior is evidently related with different sizes and dispersion of ZnO species present in the materials.

Thus, according to the characterization results shown, the oxide species for the samples with lower Zn contents would be finely dispersed on the silica structure and active for the photodegradation. In contrast, the samples with high metal contents present oxides of higher size, which could be blocking some active sites.

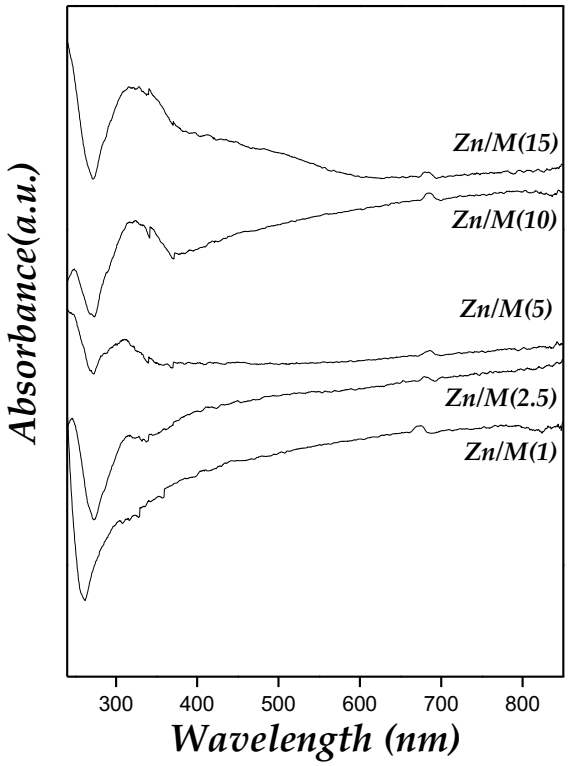

Fig. 5. DRUV-vis spectra of the Zn/MCM-41 synthesized samples.

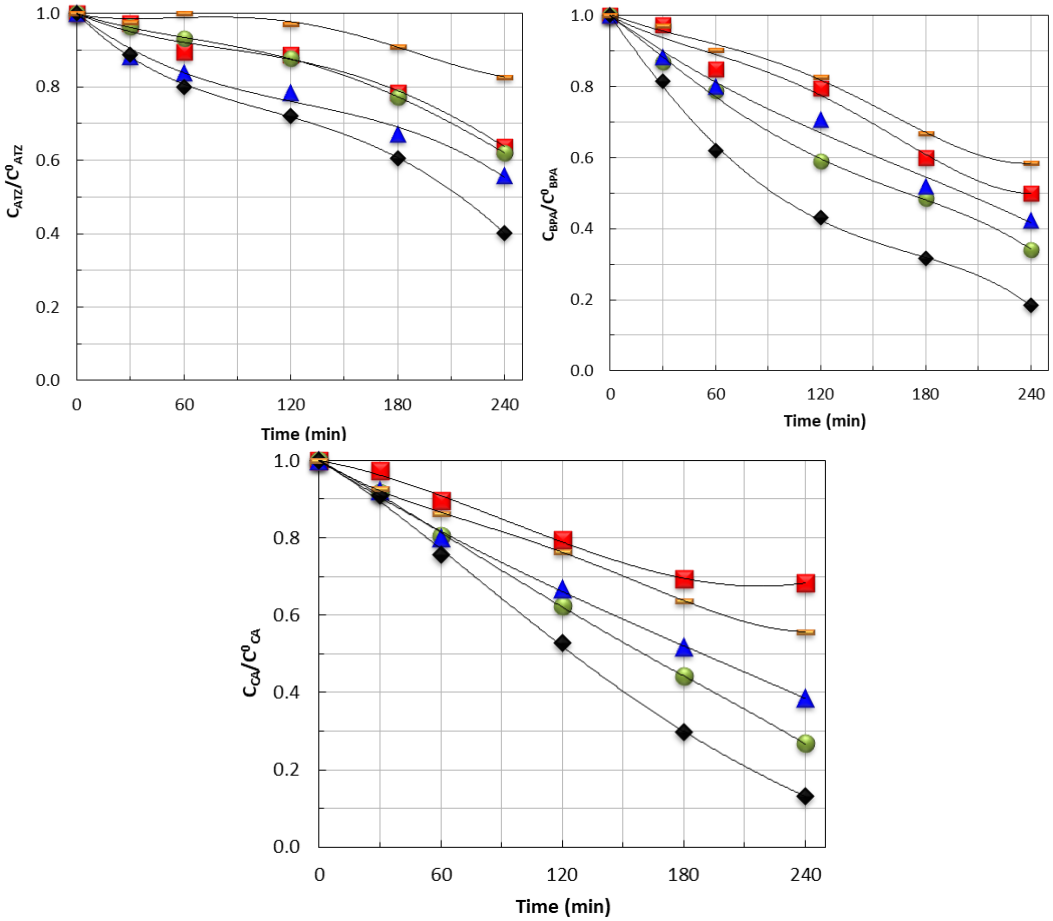

Fig. 6. Relative pollutants concentration as a function of time, for heterogeneous photo-Fenton processes: Zn/M(1) (■), Zn/M(2.5) (●), Zn/M(5) (♦), Zn/M(10) (▲) and Zn/M(15) (–) for a) ATZ b) BPA and c) CA.

Finally, in Fig. 7 are shown the measured values of the ATZ, BPA and CA degradation percentage as a function of the different Zn loadings. It can be noted that the results obtained can be viewed as a typical volcano plot, where a maximum defining the best catalyst for a given reaction, is evidenced (Boudart *et al*. 1997). This shows how the activity of different catalysts varies as a function of the Zn nominal loading. Thus, degradation percentages reached a maximum of 59.8%, 81.56% and 86.78% for ATZ, BPA and CA respectively; when the Zn content was 5 wt.%. Therefore, this Zn content would lead to a catalyst containing ZnO species with suitable dispersion and active for the degradation.

Based on these results, as can be seen, atrazine was the endocrine disruptor that caused the greatest resistance to degradation, due to the stability of the N-heterocyclic ring of this molecule (Benzaquén *et al*. 2012). Additionally, control experiments were carried out in the reactor without catalyst in order to evaluate the direct photolysis of the pollutants under the irradiation conditions employed in this study. No significant changes were detected in the concentration of ATZ, BPA and CA after 240 min of irradiation.

In addition, in order to check the zinc leaching to the reaction medium, ICP measurements of the filtered reaction mixture after 6 h of radiation were carried out. The Zn leaching values were around 0.5 mg L^{-1} from Zn/M(5) catalyst during heterogeneous photo-Fenton degradation of ATZ, BPA and CA. Nevertheless, it is important to mention that the solid synthesized here (Zn/M(5)) could be re-used even after three cycles without loss of activity (Table 3). Therefore, it is clearly evidenced that the active Zn species were efficiently retained on the mesoporous surface.

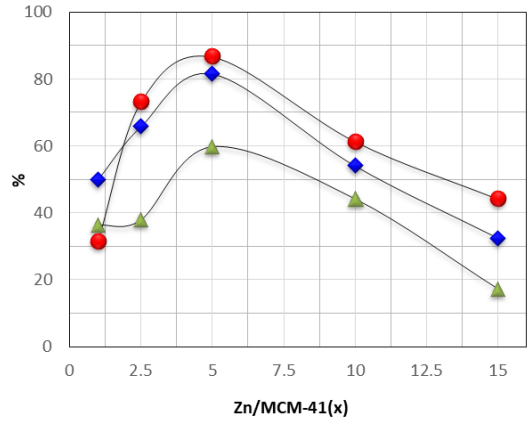

Fig. 7. Volcano plots after 240 min, for all samples modified with Zn, C^0_{CAT}= 1 g L^{-1}, for the degradation of ATZ (▲) BPA (◆) and CA (●).

Therefore, taking the above results into consideration, a low Zn loading on our MCM-41 materials would lead to an efficient photocatalyst for the degradation of these endocrine disruptors.

Conclusions

Zn/MCM-41 molecular sieves were successfully prepared by wet impregnation with $Zn(NO_3)_2 \bullet 6H_2O$ as zinc source, for pollutants degradation by means the heterogeneous photo-Fenton process.

All of the materials presented high S_{BET}, pore volume and ordered structure after the Zn incorporation. The high Zn contents affected the pore structure and the textural properties of these materials, leading to a structural deteriorate evidenced by XRD and N_2 isotherms at 77 K. The heterogeneous photo-Fenton degradation of endocrine disruptors (such as atrazine, clofibric acid and bisphenol) using Zn/MCM-41 catalysts has been successfully tested. It is important to remark that the heterogeneous reaction was carried out at near-neutral natural pH and with a low consumption of hydrogen peroxide. The mesostructure containing 5 wt.% of Zn presented the higher pollutant degradation, reaching a maximum of 59.8%, 81.56% and 86.78% for ATZ, BPA and CA respectively. It was found that the Zn species responsible for the activity would be ZnO small species, highly dispersed and interacting with the support surface, which were evidenced by XPS and UV-vis. When the Zn loading increased, the Zn species increased in amount and size, probably blocking active sites on the support. This material could be re-used even after various cycles without loss of activity.

Thus, Zn/MCM-41 materials are proposed as an important alternative for use as photocatalysts in the pollutants degradation in water.

Acknowledgements

This work was supported by Universidad Tecnológica Nacional (UTN-FRC); Universidad Nacional de Córdoba, Universidad Nacional del Litoral (UNL) and Consejo Nacional de Investigaciones Científicas (CONICET).

References

Allen A., Hochanadel C., Ghormley J., Davis J. (1952). Decomposition of water and aqueous solutions under mixed fast neutron and γ-radiation. *Journal of Physical Chemistry B 56*, 575-586.

Ansari S.A., Khan M.M., Ansari M.O., Lee J., Cho M.H. (2013). Biogenic synthesis, photocatalytic, and photoelectrochemical performance of Ag-ZnO nanocomposite. *Journal of Physical Chemistry C 117*, 27023-27030.

Bengoa J., Cagnoli M., Gallegos N., Alvarez A., Mogni L., Moreno M., Marchetti S. (2005). Iron oxide nanoparticles inside the MCM-41 channels: Study of the structural stability of the support. *Microporous and Mesoporous Materials 84*, 153-160.

Benzaquén T.B., Islaa M.A., Alfano O.M. (2012). Quantum efficiencies of the photo-Fenton degradation of atrazine in water. *Water Science and Technology 66*, 2209-2216.

Benzaquén T.B., Benzzo M.T., Isla M.A., Alfano O.M. (2013). Impact of some herbicides on the biomass activity in biological treatment plants and biodegradability enhancement by a photo-Fenton process. *Water Science and Technology 67*, 210-216.

Benzaquén T.B., Islaa M.A., Alfano O.M. (2015). Combined chemical oxidation and biological processes for herbicide degradation. *Chemical and Technological Biotechnology 90*, 459-467.

Benzaquén T.B., Cuello N.I., Alfano O.M., Eimer G.A. (2017). Degradation of Atrazine over a heterogeneous photo-fenton process with iron modified MCM-41 materials. *Catalysis Today 296*, 51-58.

Boudart M., Ertl G., Knözinger H., Weitkamp J. (1997). *Handbook of Heterogeneous Catalysis*. Wiley-VCH, Weinheim 1.

Brunauer S., Emmett P.H., Teller E. (1938). Adsorption of gases in multimolecular layers. *Journal of the American Chemical Society 60*, 309-339.

Carlson T. A. (1975). *Photoelectron and Auger Spectroscopy*. Plenum Publishing Corporation, New York.

Carraro P.M., Elías V.R., García Blanco A.A., Sapag K., Moreno S., Oliva M.I., Eimer G.A. (2014). Synthesis and multi-technique characterization of nickel loaded MCM-41 as potential hydrogen-storage materials. *Micropor. Mesopor. Mater. 191*, 103-111.

Chandrappa K. G. and Venkatesha T. V. (2012). Electrochemical synthesis and photocatalytic property of zinc oxide nanoparticles. *Nano-Micro Lett. 4*, 14-24.

Chen H.G., Shi J.L., Chen H.R., Yan J.N., Li Y.S., Hua Z.L., Yang Y., Yan D.S. (2004). The preparation and photoluminescence properties of ZnO-MCM-41. *Optical Materials 25*, 79-84.

Chu W., Chan K. H., Kwan C.Y., Choi K.Y. (2007). Degradation of atrazine by modified stepwise-Fenton's processes. *Chemosphere 67*, 755-761.

Diamanti-Kandarakis E., Bourguignon J-P, Giudice L.C., Hauser R., Prins G.S., Soto A.M., Zoeller R.T., Gore A.C. (2009). Endocrine-disrupting chemicals: an endocrine society scientific statement. *Endocrine Reviews 30*, 293-342.

Do Y., Kim J., Park J., Park S., Hong S., Suh C., Lee G. (2005). Photocatalytic decomposition of 4-Nitrophenol on Ti-containing MCM-41. *Catalysis Today 101*, 299-305.

Dordio A., Estêvão Candeias A., Pinto A., Teixeira da Costa C., Palace Carvalho A. (2009). Preliminary media screening for application in the removal of clofibric acid, carbamazepine and ibuprofen by SSF-constructed wetlands. *Ecology Engineering 35*, 290-302

Dupin J-C, Gonbeau D., Vinatier P., Levasseur A. (2000). Systematic XPS studies of metal oxides, hydroxides and peroxides. *Physical Chemistry and Chemical Physics 2*, 1319-1324.

Elías V., Crivello M., Herrero E., Casuscelli S., Eimer G. (2009). Some considerations to optimize the synthesis procedure and the structural quality of mesostructured silicas. *Journal of Non-Crystaline Solids 355*, 1269-1273.

Elías V., Sabre E., Winkler E., Satuf M., Rodriguez-Castellón E., Casuscelli S., Eimer G. (2012). Chromium and titanium/chromium-containing MCM-41 mesoporous silicates as promising catalysts for the photobleaching of azo dyes in aqueous suspensions. A multitechnique investigation. *Microporous and Mesoporous Materials 163*, 85-95.

Esplugas S., Bil D.M., Krause L. G. T., Dezotti M. (2007). Ozonation and advanced oxidation technologies to remove endocrine disrupting chemicals (EDCs) and pharmaceuticals and personal care products (PPCPs) in water effluents. *Journal of Hazardous Materials 149*, 631-642.

Everett D.H. (1971). *Manual of Symbols and Terminology for Physicochemical Quantities and Units Appendix II. Definitions, Terminology and Symbols in Colloid and Surface Chemistry*. Part I. (IUPAC).

García Blanco A. A., Amaya Ma. G., Roca Jalil Ma. E., Nazzarro M., Oliva M. I., Sapag K. (2011). Effect of the synthesis method on co-catalysts based on MCM-41 for the Fischer-Tropsch reaction. *Topics in Catalysis 54*, 190-200.

Huang N., Shu J.X., Wang Z.H., Chen M., Ren C.G., Zhang W. (2015). One-step pyrolytic synthesis of ZnO nanorods with enhanced photocatalytic activity and high photostability under visible light and UV light irradiation. *Journal of Alloys Compounds 648*, 919-929.

Huang Y., Wong C., Zheng J., Bouwman H., Barra R., Wahlström B., Neretin L., Wong M. (2011). Bisphenol A (BPA) in China: A review of sources, environmental levels, and

potential human health impacts. *Environmental International 42*, 91-99.

Jiang Q., Wu Z.Y., Wang Y.M., Cao Y., Zhou C.F., Zhu J.H. (2006). Fabrication of photoluminescent ZnO/SBA-15 through directly dispersing zinc nitrate into the as-prepared mesoporous silica occluded with template. *Materials Chemistry 16*, 1536-1542.

Jones C. W. (1999). *Applications of Hydrogen Peroxide and Derivatives*. The Royal Society of Chemistry: Cambridge.

Lee H.J., Kim J.H., Park S.S., Hong S.S., Lee G.D. (2015). Degradation kinetics for photocatalytic reaction of methyl orange over Al-doped ZnO nanoparticles. *Industrial and Engineering Chemistry 25*, 199-206.

Lihitkar P.B., Violet S., Shirolkar M., Singh J., Srivastava O.N., Naik R.H., Kulkarni S.K. (2012). Confinement of zinc oxide nanoparticles in ordered mesoporous silica MCM-41. *Materials Chemistry and Physics 133*, 850-856.

Liotta L. F., Gruttadauria M., Di Carlo G., Perrini G., Librando V. (2009). Heterogeneous catalytic degradation of phenolic substrates: catalysts activity. *Journal of Hazardous Materials 162*, 588-606.

Litter M.I. (2005). Introduction to photochemical advanced oxidation processes for water treatment. In: *Environmental Photochemistry Part II. The Handbook of Environmental Chemistry*, vol 2M (Boule P., Bahnemann D.W., Robertson P.K.J. eds) Springer, Berlin, Heidelberg.

Manassero A., Satuf M.L., Alfano O.M. (2013). Evaluation of UV and visible light activity of TiO_2 catalysts for water. *Chemical Engineering Journal 225*, 378-386.

Mihai G. D., Meynen V., Mertens M., Bilba N., Cool P., Vansant E. F. (2010). ZnO nanoparticles supported on mesoporous MCM-41 and SBA-15: a comparative physicochemical and photocatalytic study. *Journal of Materials Science 45*, 5786-5794

Murov S.L., Carmichael I., Hug G.L. (1993). *Handbook of Photochemistry*, 2nd edition, (Marcel Dekker, ed.) New York.

Pignatello J. J., Oliveros E., MacKay A. (2006). Advanced oxidation processes for organic. contaminant destruction based on the Fenton reaction and related chemistry. *Critical Reviews in Environmental Science and Technology 36*, 1-84.

Ravikovitch P.I., Neimark A.V. (2001). Characterization of nanoporous materials from adsorption and desorption isotherm. *Colloid Surfaces A 11*, 187-188

Rouquerol F., Rouquerol J., Sing K. (1999) In: *Adsorption by Powders and Porous Solids, Principles, Methodology and Applications*.

Savidha R., Pandurangan A. (2004). Vapour phase isopropylation of phenol over zinc- and iron-containing Al-MCM-41 molecular sieves. *Applied Catalysis A: General 262*, 1-11.

Shen S., Chen J., Koodali R.T., Hu Y., Xiao Q., Zhou J., Wang X., Guo L. (2014). Activation of MCM-41 mesoporous silica by transition-metal incorporation for photocatalytic hydrogen production. *Applied Catalysis B Environment 150-151*, 138-146.

Tixier C., Singer H. P., Oellers S., Müller S. R. (2003). Occurrence and fate of carbamazepine, clofibric acid, diclofenac, ibuprofen, ketoprofen, and naproxen in surface waters.*Environmental Science and Technology 37*, 1061-1068.

Torres-Otánez, G. *et al*. (2017). Preparation and evaluation of NiCoMo hydrodesulfuration catalysts supported over a binary zeolite(beta)-KIT-6 siliceous material. *Revista Mexicana de Ingeniería Química 17*, 215-228.

US Environmental Protection Agency (USEPA) (2001). *Memorandum: Atrazine. HED Product and Residue Chemistry Chapters. Office of Prevention, Pesticides and Toxic Substances*, Washington, DC.

Vaschetto, E.G.; Casuscelli, S.G.; Eimer, G.A (2018). B-MCM-41 as nano-structured catalysts for the improvement of Beckmann reaction conditions. *Revista Mexicana de Ingeniería Química 17*, 633-640.

Zhang W-H, Shi J-L, Wang L-Z, Yan D-S (2000). Preparation and characterization of ZnO clusters inside mesoporous silica. *Chemical Materials 122*, 1408-1413.